The site and local environment of Fe^{3+} in $LiNbO_3$ investigated with ENDOR

1992 J. Phys.: Condens. Matter 4 9901

(http://iopscience.iop.org/0953-8984/4/49/017)

J. Phys.: Condens. Matter 4 (1992) 9901–9908. Printed in the UK

The site and local environment of Fe^{3+} in $LiNbO_3$ investigated with ENDOR

H Söthe and J-M Spaeth

Universität Paderborn, Fachbereich Physik, Warburgerstraße 100, D-4790 Paderborn, Federal Republic of Germany

Received 17 August 1992, in final form 30 September 1992

Abstract. The superhyperfine (SHF) interactions of Fe^{3+} impurities with five shells of Li neighbours were measured in a nearly stoichiometric $LiNbO_3$ crystal by applying electron nuclear double resonance (ENDOR). Similarly to what was found for $LiTaO_3$, the site of Fe^{3+} in $LiNbO_3$ has a threefold symmetry. The analysis of the ENDOR spectra clearly shows that Fe^{3+} is on a substitutional Li^+ site. The variations of shape and intensity of ENDOR lines belonging to specific ligand nuclei when rotating the crystal in the static magnetic field are attributed to local disorder.

1. Introduction

The photorefractive effect in $LiNbO_3$ is known to be correlated to the presence of transition metal impurities (Line and Glass 1977, Kurz *et al* 1977, Krätzig and Orlowski 1978) and to the non-stoichiometric nature of most crystals. For the photorefractive effect in particular, Fe^{3+} dopants play a key role. For a better understanding of the photorefractive effect a precise knowledge of the defect structure of Fe^{3+} impurities in $LiNbO_3$ is needed. In spite of many attempts to determine the location of Fe^{3+} by experiments (Mehran and Scott 1972, Pechenyl 1984, Grachev and Malovichko 1985) applying optical and electron spin resonance (ESR) spectroscopy as well as by theory (Agullo-Lopez and Müller 1987), the results were not clear beyond doubt. A Li^+ substitutional site with C_3 symmetry is also discussed as a substitutional Nb^{5+} site which seems to be favoured from Mössbauer investigations (Keune *et al* 1976). Recently, the site of Fe^{3+} in $LiNbO_3$ was also studied by EXAFS (Catlow *et al* 1991) and PIXE channelling experiments (Rebouta *et al* 1991). It was found that Fe^{3+} substitutes for Li^+. In order to apply these two methods the dopant concentration must be of the order of 1% or even higher. But for such high concentrations the Fe^{3+} site may be different from that occupied at lower concentrations which are those relevant to most applications.

The site of a paramagnetic defect can also be determined by electron nuclear double resonance (ENDOR). ENDOR spectra yield superhyperfine (SHF) and quadrupole tensors for magnetic nuclei surrounding the paramagnetic defect, from the analysis of which a clear defect model can often be derived. The measured quadrupole interactions give additional information about the local electric field gradients.

In this paper we present an ENDOR study of Fe^{3+} in a $LiNbO_3$ crystal, which was almost stoichiometric. Attempts to measure ENDOR in congruent $LiNbO_3$ failed, as

0953-8984/92/499901+08$07.50

reported earlier (Söthe *et al* 1989). We confirm the Li^+ site for Fe^{3+}, but also find that there is some local disorder amongst the near neighbours of this site.

2. Experimental details

The 'stoichiometric' crystal was grown in air at the Research Laboratory for Crystal Physics of the Hungarian Academy of Science, Budapest, starting with a Li/Nb ratio of 1.1 : 1 in the melt. The concentration of the Fe^{3+} dopant was 0.02 mol%. ESR and ENDOR experiments were performed in a custom-built computer-controlled X-band spectrometer (9.3 GHz). The magnetic field could be varied from 50 to 1150 mT. The sample was cooled in a helium cryostat, the temperature of which could be stabilized anywhere between room temperature and about 3.5 K. Stationary ENDOR was performed in the frequency range 0.5–160 MHz. The recorded spectra were digitally filtered. Deconvolution algorithms and special peak-search algorithms were applied in order to determine the ENDOR line positions (Niklas 1983).

3. Experimental results

3.1. Electron spin resonance (ESR)

The angular dependence of the Fe^{3+} ESR spectrum in $LiNbO_3$ is shown in figure 1. It was measured for a rotation of the $LiNbO_3$ crystal in a plane perpendicular to its optical axis (c-axis). The angular dependence was analysed using an axially symmetric spin Hamiltonian for a $3d^5$ configuration ($S = \frac{5}{2}$, $^6S_{5/2}$) and the major crystal-field term B_2^0 (Abragam and Bleaney 1970). The axial symmetry axis z is parallel to the c-axis of the crystal.

$$H = \beta_e \boldsymbol{B} \cdot \tilde{\mathbf{g}} \cdot \boldsymbol{S} + 3B_2^0(S_z^2 - \tfrac{35}{12}) \tag{1}$$

The electron Zeeman interaction is described in the first term of the Hamiltonian. The second term represents the fine structure where $3B_2^0$ is the crystal-field parameter, the other symbols having their usual meaning. From earlier ESR investigations of Fe^{3+} in $LiNbO_3$ it is known that the fine structure term is of the same order of magnitude as the electron Zeeman term (Mehran and Scott 1972, Towner *et al* 1972). Thus the Hamiltonian (1) has to be diagonalized numerically. In figure 1 the squares represent the ESR line positions, while the solid 'lines' (+) were calculated using the Hamiltonian (1) with an isotropic g-value of $g = (1.995 \pm 0.003)$ and a crystal field parameter of $3B_2^0 = (5440 \pm 150)$ MHz. Due to the small difference between the fine structure and the electron Zeeman energy the calculated ESR angular dependence has a complicated pattern. Similarly, as in the case of Fe^{3+} in $LiTaO_3$ (Söthe *et al* 1989), 'loops' appear in the angular dependence. When analysing the ESR spectra, the same problems were met as with Fe^{3+} in $LiTaO_3$: the ESR lines have large linewidths and unusual line shapes. Because of the broad ESR linewidths only the first-order terms of the ESR Hamiltonian were taken. Corrections due to small higher-order crystal-field terms were neglected because of the uncertainty in the first-order terms due to the large linewidths. Apart from the ESR lines of the Fe^{3+} dopants some weaker ESR lines of unknown origin were found.

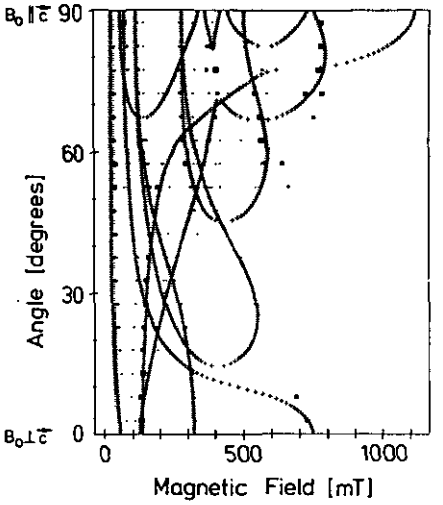

Figure 1. Angular dependence of the Fe^{3+} ESR spectrum in $LiNbO_3$ for a rotation of the magnetic field from $B_0 \parallel c = 90°$ to $B_0 \perp c = 0°$. $T = 10$ K, $\nu = 9.35$ GHz. (□) represents the ESR line positions, their size is a measure of their linewidths. + is the calculated ESR angular dependence (see text).

3.2. Electron nuclear double resonance (ENDOR)

Stationary ENDOR experiments (Seidel 1961) were performed by partially saturating the high-field ESR transition with the magnetic field B_0 in a plane perpendicular to the crystal c-axis. Due to the axially symmetric fine-structure tensor, the ESR line remains at constant field when rotating the crystal about its c-axis. In figures 2 (*a*) and (*b*) typical ENDOR spectra are shown for two orientations of the magnetic field perpendicular to the c-axis. As was found previously for all other impurities investigated in $LiNbO_3$ there is a rather large structureless 'background' in the ENDOR spectrum, which decreases with increasing frequency. In all the Fe^{3+}-doped congruent $LiNbO_3$ samples investigated only this structureless ENDOR effect could be found. Only in 'stoichiometric' samples were sharp ENDOR lines observed. Figure 3 shows the angular dependence of the sharp ENDOR lines. The dots in the angular dependence represent the ENDOR line positions when rotating the crystal about its c-axis from $B_0 \parallel x$ to $B_0 \parallel y$ (see figure 4). For these measurements the ESR transition at 730 mT was saturated. Two separate line groups can be seen around the Larmor frequencies of ^{93}Nb ($\nu_n = 7.63$ MHz) and of ^{7}Li ($\nu_n = 12.08$ MHz). No other ENDOR lines than those in figure 3 were found up to a frequency of 160 MHz. ENDOR lines due to oxygen and iron nuclei cannot be expected because of the low abundance of the magnetic isotopes ^{17}O and ^{57}Fe.

The spin Hamiltonian describing the ENDOR transitions including SHF interactions is

$$H = \beta_e B \cdot \tilde{\mathbf{g}} \cdot S + 3B_2^0(S_z^2 - \tfrac{35}{12}) + \sum_{i=1}^{N}(S A_i I_i - g_{I,i}\beta_n I_i B + I_i Q_i I_i) \qquad (2)$$

This spin Hamiltonian consists of equation (1) and the nuclear spin Hamiltonian. The sum in the nuclear spin Hamiltonian runs over all nuclei having a SHF interaction with the Fe^{3+}. A_i is the SHF interaction tensor of a nucleus i in the neighbourhood of the paramagnetic defect. $g_{I,i}$ is the nuclear g-factor of the nucleus i. The term $I_i Q_i I_i$ in the sum represents the quadrupole interaction, which may occur for nuclei with $I > \frac{1}{2}$. The other symbols have their usual meanings.

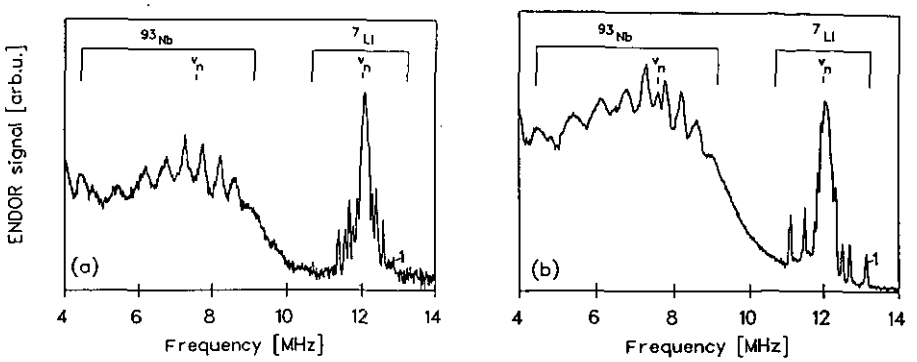

Figure 2. (*a*) ENDOR spectrum for $B_0 \parallel y$ (see figure 4), $B_0 = 730$ mT, $T = 4.5$ K. The spectrum contains ^{7}Li and ^{93}Nb ENDOR lines around their respective Larmor frequencies. (*b*) ENDOR spectrum for $B_0 \parallel x$ (see figure 4), $B_0 = 730$ mT, $T = 4.5$ K.

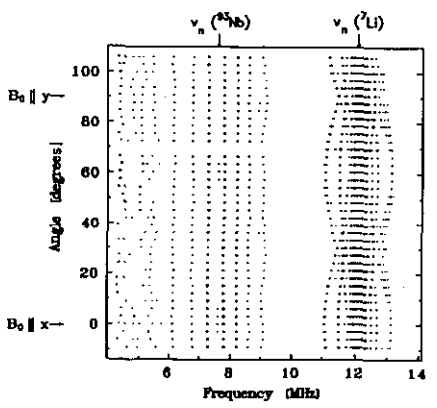

Figure 3. ENDOR angular dependence of all observed sharp ENDOR lines measured at $T = 4.5$ K when rotating the crystal from $B_0 \parallel x$ to $B_0 \parallel y$ perpendicular to the c-axis.

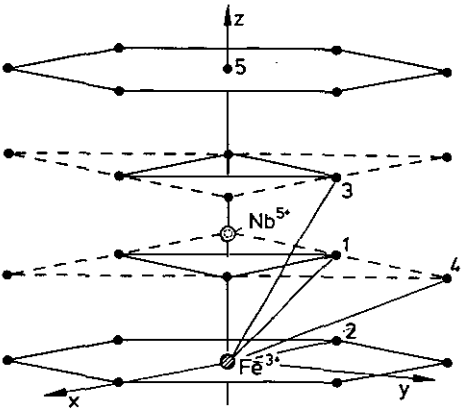

Figure 4. Schematic representation of the Li sublattice. The numbers represent the Li shells with increasing distance from the Fe^{3+} impurity which is assumed to be on a substitutional Li site. The on-axis Nb position is indicated as an open circle.

The ENDOR lines measured in the region around the Larmor frequencies of ^{93}Nb are due to quadrupole transitions of ^{93}Nb ($I = \frac{9}{2}$, natural abundance: 100%). In the group of ENDOR lines around the Larmor frequency of ^{7}Li no resolved quadrupole lines were observed; all lines are due to ^{7}Li SHF interactions. In order to calculate the ENDOR frequencies the electron Zeeman and the fine-structure term were diagonalized numerically first. With the result of this diagonalization the effective spin quantum number m_{seff} was calculated as the expectation value of the z-component of the electron spin. The effective spin m_{seff} is a function of the fine structure parameter B_2^0 and of the magnetic field B_0 where the ESR is saturated. The effective spin quantum number m_{seff} is then set into the nuclear spin Hamiltonian, the third term in equation (2). The nuclear spin Hamiltonian had to be diagonalized within the nuclear quantum states. The ENDOR frequencies are given in a first-order

solution by

$$\nu_i = (1/h)|m_{seff}(B_0, B_2^0)A_i(\theta_i, \psi_i, \phi_i) + Q_i(\theta_i, \psi_i, \phi_i) - g_{I,i}\beta_n B_0| \quad (3)$$

In this equation $A_i(\theta_i, \psi_i, \phi_i)$ is the SHF interaction energy which depends on the orientation of the SHF tensor with respect to the magnetic field and defect centre. From the ESR analysis with $3B_2^0 = 5440$ MHz and $B_0 = 730$ mT two effective spin quantum numbers $m_{seff} = 2.33$ and $m_{seff} = 1.35$ were obtained. The ESR transition at 730 mT occurs between the Zeeman levels characterized by these two m_{seff} values.

The chemical identity of a nucleus is described by the nuclear g-factor g_I. This g_I-factor can be determined from the variation of the ENDOR frequencies when measuring ENDOR at different magnetic fields within the ESR transition. This variation is approximately proportional to the field shift. With such ENDOR field shift experiments it was shown that all the ENDOR lines around $\nu_n(^{93}\text{Nb})$ belong to ^{93}Nb and all lines around $\nu_n(^7\text{Li})$ belong to ^{7}Li nuclei.

The ^{7}Li ENDOR angular dependence shows a 60° symmetry which indicates that the Fe^{3+} impurity is located on the c-axis of the crystal. Such a position on the optical axis was already indicated by the angular dependence of the ESR lines.

The ^{7}Li ENDOR angular dependence is very similar as that reported for Fe^{3+} in $LiTaO_3$ (Söthe *et al* 1989) and was analysed accordingly. As in $LiTaO_3$ the SHF interactions measured are almost entirely anisotropic SHF interactions given by the classical point dipole–dipole interaction:

$$b_{dd} = \mu_0 g_e \beta_n g_I \beta_n / 4R^3 \quad (4)$$

where R is the distance between the point dipole of the unpaired electron and the magnetic nucleus. The other symbols have their usual meaning.

Table 1 lists the distances for the first five shells of Li ligands for the assumptions that Fe^{3+} is on a Li-position (figure 4).

In figure 4 only the Li sublattice and the on-axis Nb site is drawn. From the distances from the Fe^{3+} centre to the Li nuclei, the dipole–dipole interactions were calculated using equation (4). They are also listed in table 1.

Table 1. Experimental SHF and quadrupole interaction constants (in MHz) for the Li^+ and Nb^{5+} shells around the Fe^{3+} impurity in stoichiometric $LiNbO_3$. The SHF interaction constants are defined in equation (5). For comparison, the anisotropic SHF constant b is calculated with the point dipole–dipole approximation: b_{dd}. n denotes the number of nuclei in each shell. Also the distances between the Li neighbour shells from Fe^{3+} being on a Li site (in Å) are included.

	Shell	n	a/h	b/h	b_{dd}/h	q/h	$\lvert a-b\rvert/h$	Distance Li^+–Fe^{3+}
Li	1	3	0.10*	0.55*	0.57*			3.76
	2	6	0.01	0.22	0.22			5.15
	3	3	0.02	0.20	0.19			5.49
	4	3	0.01	0.12	0.12			6.38
	5	1	—	—	0.09		0.09	6.93
Nb on c-axis						0.16	0.02	

* Precision only ±0.03 MHz.

The z-axis of the SHF tensor is the connection line between the Fe^{3+} and the ligands (see figure 4). The experimental error is +0.015 MHz.

The ENDOR angular dependence of the ^{7}Li lines (assuming a point dipole–dipole interaction for the case where the Fe^{3+} is on a Nb site) is plotted in figure 5 as solid lines. For this Fe^{3+} site the first and the fourth shell of Li neighbours should lead to an isotropic line in the angular dependence when rotating the sample about the c-axis. These were not found.

Figure 6 shows the calculated ENDOR angular dependence using equation (4) for the assumption that the Fe^{3+} is on a Li site. The first four shells of Li neighbours can be separated into one set of shells (first, third and fourth shell) where the Li nuclei lie on the y-axis of the crystal, and one shell where there are nuclei on the x-axis (figure 4).

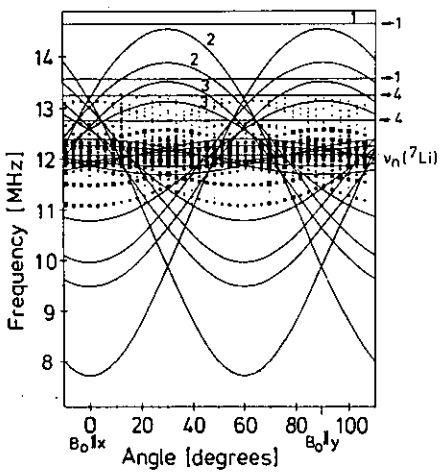

Figure 5. ENDOR angular dependence of the Li ENDOR spectrum. The sample was rotated in a plane perpendicular to the c-axis. (□) represents measured ENDOR line positions. (——) are calculated assuming that the SHF interaction is given by the point dipole–dipole interaction for the Fe^{3+} on a substitutional Nb site.

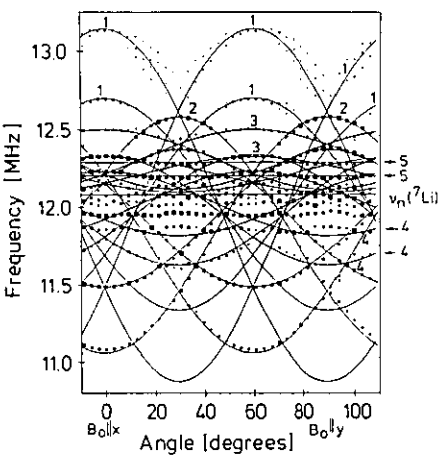

Figure 6. ENDOR angular dependence of the Li ENDOR spectrum for a sample rotation in a plane perpendicular to the c-axis. (□) represents the measured ENDOR line positions. (——) are calculated with the SHF-interaction parameters listed in table 1 for the assumption that the Fe^{3+} occupies a substitutional Li^+ site. The Li shells are indicated by numbers according to figure 4.

Therefore the branches of the second shell are 30° shifted relative to the branches of all the other shells. As can be seen in this figure the calculated angular dependence explains the measured ENDOR lines very well. Due to line-broadening effects (see below) not enough ENDOR lines could be measured for as precise a determination of the SHF interaction parameters of the first shell neighbours as for the other shells. In table 1 the SHF parameters determined from the best fit to the experimental data are listed in terms of the isotropic SHF parameter a and the anisotropic SHF parameter b. The isotropic and anisotropic SHF parameters are related to the principal values of the SHF tensor **A** by

$$a = \tfrac{1}{3}(A_{xx} + A_{yy} + A_{zz}) \tag{5}$$

$$b = \tfrac{1}{2}(A_{zz} - a)$$

The isotropic SHF parameters were found to be negligibly small, only in the first shell there is a small isotropic constant. Comparison of the anisotropic SHF parameter b with the point dipole–dipole values b_{dd} show that the SHF interacting can indeed be described very well by assuming a point dipole on the Li^+ site interaction with the Li shells. The tensor orientations are always assumed to be the connection lines between ligands and Li^+ site. The ^{93}Nb lines detected are due to nuclei on the c-axis because of the isotropic pattern in the angular dependence. For these lines the SHF interaction is very small ($|a - b| \simeq 20$ kHz). Obviously the ENDOR lines must be attributed to a Nb nucleus on the c-axis. No other ^{93}Nb lines were found. The occurrence of 9 Nb ENDOR lines (figures 2 and 3) for each m_{seff} is due to a small quadrupole interaction ($I = \frac{9}{2}$) (see table 1).

4. Discussion

From the calculated ENDOR angular dependence the Nb site for the Fe^{3+} impurity can be excluded. All other off-centre positions for Fe^{3+} on the c-axis can also be excluded, since different ENDOR angular dependences would be expected (see figure 5 in Corradi *et al* 1990). Therefore our analysis clearly shows that Fe^{3+} in $LiNbO_3$ must occupy a substitutional Li^+ site.

The SHF interactions of five Li^+ shells can be explained by a point dipole–dipole interaction within experimental error. Similarly as in the case of Fe^{3+} in $LiTaO_3$ (Söthe *et al* 1989) or Mn^{2+} in $LiNbO_3$ (Corradi *et al* 1990) there is apparently only very little overlap transfer from the $3d^5$ orbitals via the oxygen neighbours to the Li shells. This results in the observed small isotropic SHF interactions.

In the measured Li ENDOR angular dependence a strong line-broadening can be seen when following the first-shell Li^+ lines from $B_0 \parallel x$ to $B_0 \parallel y$. In figure 2 the ENDOR spectra for $B_0 \parallel y$ (figure 2 (a)) and $B_0 \parallel x$ (figure 2 (b)) are plotted. The first-shell Li lines are at about 13.1 MHz for $B_0 \parallel x$ and at about 12.7 MHz for $B_0 \parallel y$ (see lines marked by 1 in figures 2 (a) and (b)). In figure 2 (b) the ENDOR lines are relatively sharp. When measuring the angular dependence the ^7Li lines broaden beyond recognition within about 40°. For $B_0 \parallel x$ the magnetic field is perpendicular to the SHF z-axis of some first-shell nuclei, i.e. one measures $A_\perp = |a - b|$. If the first-shell Li ligand position varies somewhat due to a lattice imperfection caused by other nearby defects, then the z-axes orientation relative to the c-axis of the crystal of the SHF tensors may vary and thus the SHF interaction results in line-broadening effects. These effects are minimal for B_0 perpendicular to the z-axis, since the SHF interaction varies like $3\cos^2\theta - 1$, where θ is the angle between B_0 and z. Therefore we see sharp lines for field orientations measuring approximately $A_\perp$ and broad lines for B_0 having smaller angles with the z-axes of the Li SHF tensors. A significant variation of the linewidth was also observed for the second-shell ligands. Our observations indicate that the environment of the Li site occupied by Fe^{3+} is not perfect. There must be local disorder which may be caused by nearby charge-compensating defects. This corroborates with the failure to see sharp Fe^{3+} ENDOR lines in congruent crystals, although the EPR spectra of Fe^{3+} could be measured and the ENDOR effect was indeed present. We think that all Li ENDOR lines were broadened there beyond recognition. This is qualitatively the same behaviour as discussed for Mn^{2+} on Li sites in $LiNbO_3$ (Corradi *et al* 1990). Except for the first shell all other observed ENDOR lines are detectable across the

complete angular range. The smaller linewidth variations of ENDOR signals due to outer-shell Li^+ nuclei (shells 2, 3, 4, 5) can in principle be explained by unresolved quadrupole splittings ($I(^7Li) = \frac{3}{2}$) or small effects of disorder. In $LiNbO_3$ there are two inequivalent Li sites (or any other on-axis sites) with different orientations of the surrounding oxygen octahedra. The two kinds of sites are connected by y–z glide planes. If the Fe^{3+} was shifted from the Li site to any direction on the c-axis, the glide-plane symmetry would be broken. Then all Li shells would split into two subshells with different SHF parameters. This was not observed. From the ENDOR linewidth of the unsplit third shell an upper limit for a possible displacement was estimated to be $|d| \leqslant 0.05$ Å. This estimate is based on the point dipole–dipole interpretation of the SHF interaction in the third shell which explains the experimental angular dependence excellently.

5. Conclusion

It was shown that Fe^{3+} substitutes for Li^+ in stoichiometric $LiNbO_3$. From an analysis of the observed width of the ENDOR lines it is estimated, that the Fe^{3+} impurity is displaced from the Li lattice site by less than 0.05 Å along the c-axis. Due to the strong angle-dependent broadening of the first-shell Li lines it is concluded that there must be local disorder, possibly caused by charge compensating defects.

Acknowledgment

We would like to thank G Corradi for helpful discussions and the almost stoichiometric $LiNbO_3$:Fe^{3+} crystal.

References

Abragam A and Bleaney B 1970 *Electron Paramagnetic Resonance of Transition Ions* (Oxford: Clarendon)
Agullo-Lopez F and Müller K A 1987 *Cryst. Latt. Defects Amorph. Mater.* **15** 89
Catlow C R A, Donnerberg H, Schirmer O, Tomlinson S M and Cole M *Sixth Europhysical Topical Conference, Lattice Defects in Ionic Materials (Groningen, 1990)* abstract p 225
Corradi G, Söthe H, Spaeth J-M and Polgar K 1990 *J. Phys.: Condens. Matter* **2** 6603
Grachev V G and Malovichko G I 1985 *Sov. Phys.–Solid State* **27** 424
Keune W, Date S K, Gonser U and Bunzel H 1976 *Ferroelectrics* **13** 443
Krätzig E and Orlowski R 1978 *Appl. Phys.* **15** 133
Kurz H, Krätzig E, Keune W, Engelmann H, Gonser U, Dischler B and Räuber A 1977 *Appl. Phys.* **12** 355
Line M E and Glass A M 1977 *Principles and Applications of Ferroelectrics and Related Materials* (Oxford: Clarendon)
Mehran F and Scott B A 1972 *Solid State Commun.* **11** 15
Niklas J R 1983 *Habilitationsschrift* University of Paderborn, Federal Republic of Germany
Pechenyl A P 1984 *Sov. Phys.–Solid State* **27** 923
Rebouta L, Da Silva M F, Soares J C, Hage-Ali M, Stoquert J P, Siffert P, Sanz-Garcia J A, Dieguez E and Agullo-Lopez F 1991 *Europhys. Lett.* **14** 557
Siedel H 1961 *Z. Phys.* **165** 218
Söthe H, Rowan L G and Spaeth J-M 1989 *J. Phys.: Condens. Matter* **1** 3591
Towner H H, Kim Y M and Story H S 1972 *J. Chem. Phys.* **56** 3676